

# Intrinsic finite-energy Cooper pairing in $j = 3/2$ superconductors

Masoud Bahari,<sup>1,2,\*</sup> Song-Bo Zhang,<sup>1,2</sup> and Björn Trauzettel<sup>1,2</sup>

<sup>1</sup>*Institute for Theoretical Physics and Astrophysics, University of Würzburg, D-97074 Würzburg, Germany*

<sup>2</sup>*Würzburg-Dresden Cluster of Excellence ct.qmat, Germany*

(Dated: August 4, 2021)

We show that Cooper pairing can occur intrinsically away from the Fermi surface in  $j = 3/2$  superconductors with strong spin-orbit coupling and equally curved bands in the normal state. In contrast to conventional pairing between spin-1/2 electrons, we derive that pairing can happen between inter-band electrons having different total angular momenta, i.e.,  $j = 1/2$  with  $j = 3/2$  electrons. Such superconducting correlations manifest themselves by a pair of indirect gap-like structures at finite excitation energies. An observable signature of this exotic pairing is the emergence of a pair of symmetric superconducting coherence peaks in the density of states at finite energies. We argue that finite-energy pairing is a generic feature of high-spin superconductors, both in presence and absence of inversion symmetry.

*Introduction.*—Since the discovery of the conventional Bardeen–Cooper–Schrieffer theory for superconductivity [1], extensive efforts of theoretical and experimental research have been carried out to understand the pairing mechanism [2, 3]. In most cases, superconductivity can be described by pairing of spin-1/2 electrons at the Fermi surface. However, it has been shown theoretically that pairing of electrons with higher spin degrees of freedom is indeed possible [4–6]. This has triggered attempts to formulate a general theory of high-spin superconductivity [7–10] and to identify typical physical observables [11–20]. Prominent candidate materials for high-spin superconductivity are half-Heusler compounds whose Fermi surface lies within the  $\Gamma_8$  bands of  $j = 3/2$  electrons [21–39]. These materials can be categorized into two distinct groups with inverted [21–39] and normal [29, 36, 39] band structures, respectively. In the inverted case, only a single pair of  $\Gamma_8$  bands with identical total angular momentum cross the Fermi energy [6, 40–42]. Despite the high-spin nature of electrons, the pairing mechanism in this case can be captured effectively within the formalism for (pseudo)spin-1/2 electrons at low energies [6]. In contrast, in the group with normal band structure, density functional theory calculations predict that all spin split  $\Gamma_8$  bands bend downward near the Fermi energy [22, 23, 39–42]. This band structure applies, for instance, to  $RPdBi$  with  $R \in \{Y, Dy, Tb, Sm\}$ . We demonstrate below that such configuration of energy bands in combination with superconductivity allow us to observe Cooper pairing at finite excitation energies (FEE). Interestingly, it has recently been argued that Ising superconductors may realize finite-energy pairing of spin-1/2 electrons by applying external in-plane magnetic fields [43]. Hence, the fundamental question arises whether it is possible to observe intrinsic finite-energy Cooper pairing in a superconductor in the absence of any fields.

The affirmative answer to this question is given in this Letter. We show that the interplay of strong spin-orbit coupling and multiple bands in the normal state allows pairing of electrons with *different* angular mo-

menta accompanied by a pair of indirect *gap-like structures* (GLSs) away from the Fermi energy. The electrons responsible for the finite-energy pairing originate from energy bands with different band indices (*inter-band* pairing). Our results show that such behavior is a generic feature of multiband superconductors when high-spin electrons of the  $\Gamma_8$  band contribute to pairing. In experiments, the GLSs manifest themselves by the appearance of a pair of symmetric superconducting coherence peaks at finite excitation energies of the density of states (DOS). To elucidate that finite-energy Cooper pairing is a generic phenomenon of multi-band superconductors preserving (breaking) inversion symmetry, we systematically analyze the role of high-spin pairing valid for cubic point group symmetry  $O_h$  ( $T_d$ ) based on the Luttinger-Kohn model.

*Model.*—Low-energy  $j = 3/2$  electrons within the  $\Gamma_8$  bands can be described by the  $\mathbf{k}\cdot\mathbf{p}$  Luttinger-Kohn model [44, 45],  $H_0 = \sum_{\mathbf{k}} \hat{c}_{\mathbf{k}}^\dagger \hat{H}_0(\mathbf{k}) \hat{c}_{\mathbf{k}}$ , where

$$\hat{H}_0(\mathbf{k}) = \alpha k^2 \hat{I}_4 + \beta \sum_i k_i^2 \hat{J}_i^2 + \gamma \sum_{i \neq j} k_i k_j \hat{J}_i \hat{J}_j - \mu \hat{I}_4, \quad (1)$$

and the basis is  $\hat{c}_{\mathbf{k}} = (c_{\mathbf{k},3/2}, c_{\mathbf{k},1/2}, c_{\mathbf{k},-1/2}, c_{\mathbf{k},-3/2})^T$ . We denote  $\mathbf{k} = (k_x, k_y, k_z)$  as the 3D momentum,  $k = |\mathbf{k}|$ ,  $\hat{J}_i$  with  $i \in \{x, y, z\}$  as the  $4 \times 4$  total angular momentum matrices in  $j = 3/2$  representation, and  $\hat{I}_4$  as the  $4 \times 4$  identity matrix. The material dependent parameters  $\alpha$  and  $\beta$  ( $\gamma$ ) control kinetic energy and symmetric spin-orbit coupling, respectively;  $\mu$  is the Fermi energy. The doubly-degenerate eigenenergies of  $\hat{H}_0(\mathbf{k})$ , protected by the combination of inversion and time-reversal symmetries, are given by

$$E_{\mathbf{k}}^{\pm} = \left( \alpha + \frac{5}{4} \beta \right) k^2 \pm \beta \sqrt{\sum_i \left[ k_i^4 + \left( \frac{3\gamma^2}{\beta^2} - 1 \right) k_i^2 k_{i+1}^2 \right]} - \mu, \quad (2)$$

where  $i + 1 = y$  if  $i = x$  (notation used throughout the paper). To investigate the properties of the excitation spectrum of Eq. (1) in the presence of high-spin

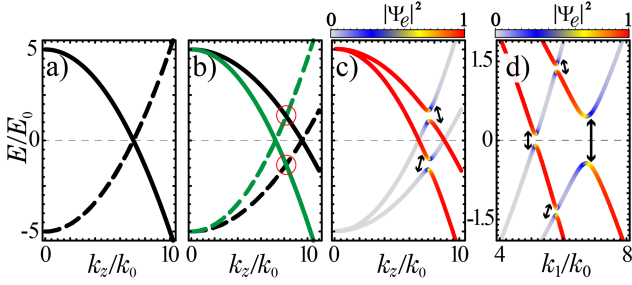


Fig. 1. BdG spectra along the two-fold rotation axis in  $[0, 0, 1]$  direction in absence of pairing for (a)  $\beta = 0$  and (b)  $\beta = 0.2|\alpha|$ , respectively. Along the two-fold rotation axes, the spectra are independent of  $\gamma$ . The solid line with black (green) color corresponds to the  $j = 3/2$  ( $j = 1/2$ ) band. The dashed lines are the hole counterparts. BdG spectrum in the (c)  $[0, 0, 1]$  and (d)  $[1, 1, 0]$  (i.e.,  $k_x = k_y = k_1$  and  $k_z = 0$ ) directions for  $\gamma = \beta$  in presence of spin-septet  $xyz$  pairing with amplitude  $\Delta/E_0a = 4.15$ . The color denotes the probability of electronic states  $|\Psi_e|^2$  in both (c) and (d) panels. Other parameters are  $\mu/E_0a^2 = -5$ ,  $k_0 = 10^{-2}a^{-1}$ ,  $E_0 = 10^{-3}|\alpha|a^{-2}$  and  $\alpha = -20$ .  $a$  is material dependent lattice constant in a tight-binding version of the continuum model.

Cooper pairing in cubic point group symmetry  $O_h$ , we introduce the full superconducting Hamiltonian given by  $H = \sum_{\mathbf{k}} \hat{\psi}_{\mathbf{k}}^\dagger \hat{H}_{\text{BdG}}(\mathbf{k}) \hat{\psi}_{\mathbf{k}}$ , where  $\hat{\psi}_{\mathbf{k}} = (\hat{c}_{\mathbf{k}}, \hat{c}_{-\mathbf{k}}^T)^T$  is the Nambu spinor. The Bogoliubov-de Gennes (BdG) Hamiltonian takes the form

$$\hat{H}_{\text{BdG}}(\mathbf{k}) = \begin{pmatrix} \hat{\mathcal{H}}_0(\mathbf{k}) & \hat{\mathcal{H}}_\eta^{J,S,L}(\mathbf{k}) \\ [\hat{\mathcal{H}}_\eta^{J,S,L}(\mathbf{k})]^\dagger & -\hat{\mathcal{H}}_0^T(-\mathbf{k}) \end{pmatrix}, \quad (3)$$

where  $\hat{\mathcal{H}}_\eta^{J,S,L}(\mathbf{k})$  is the pairing Hamiltonian in channel  $(\eta, J, S, L)$  with  $\eta$  being the relative basis label of the cubic irreducible representation (IR) [46, 47]. The channel of instability is named by Cooper-pair quantum numbers with total angular momentum  $J$  combining intrinsic spin  $S$  and orbital  $L$  angular momenta [8, 9]. A detailed description of the pairing Hamiltonian is given in the Supplemental Material [48].

To shed light on finite-energy pairing, the hole-doped BdG excitation spectrum along the  $[0, 0, 1]$  direction in absence of spin-orbit coupling and pairing is plotted in Fig. 1(a). The fourfold degenerate electron bands (solid line) cross their hole counterparts (dashed line) at  $k_F = \sqrt{\mu/\alpha}$ . A finite  $\beta$  accounting for spin-orbit coupling splits the energy bands of different spin species. Increasing  $\beta$ , this moves the crossings at the Fermi surface  $E = 0$  and at FEE (red circles), as shown in Fig. 1(b). The low-energy spin split Fermi momenta consist of  $j = 1/2$  states (green) and  $j = 3/2$  states (black) located at  $k_F^- = 2\sqrt{\mu/(4\alpha + \beta)}$  and  $k_F^+ = 2\sqrt{\mu/(4\alpha + 9\beta)}$ , respectively. Moreover, the finite-energy crossing appears at  $\tilde{k} = 2\sqrt{\mu/(4\alpha + 5\beta)}$  incorporating  $j = 3/2$  electron (hole) and  $j = 1/2$  hole (electron) states at positive (negative) excitation energies. In the superconducting state, the pairing mechanism occurs not only at  $E = 0$  but also

at FEE [Figs. 1(c) and 1(d)]. Notably, the finite-energy pairing can be present when the low-energy intra-band states exhibit nodal [Fig. 1(c)] or gapped excitation spectra [Fig. 1(d)].

*Finite-energy effective theory.*—To better understand the finite-energy pairing, we develop an effective theory close to the FEE. We start by obtaining the band basis representation of the BdG Hamiltonian through the basis transformation  $\hat{c}_{\mathbf{k}} = \hat{V}_{\mathbf{k}}^+ \hat{f}_{\mathbf{k}}^+ + \hat{V}_{\mathbf{k}}^- \hat{f}_{\mathbf{k}}^-$ , where  $\hat{V}_{\mathbf{k}}^\pm$  is a  $4 \times 2$  matrix containing the eigenvectors corresponding to  $E_{\mathbf{k}}^\pm$ . Note that  $\hat{f}_{\mathbf{k}}^\pm = (f_{\mathbf{k},\uparrow}^\pm, f_{\mathbf{k},\downarrow}^\pm)^T$  and  $f_{\mathbf{k},s}^\pm (f_{\mathbf{k},s}^\pm)^\dagger$  annihilates (creates) a state with pseudospin degrees of freedom  $s \in \{\uparrow, \downarrow\}$  in the band basis labeled by  $\pm$  in Eq. (2). To capture the inter-band superconducting Hamiltonian, we choose our basis set as  $\hat{\varphi}_{\mathbf{k}} = (\hat{\varphi}_{\mathbf{k}}^{+-}, \hat{\varphi}_{\mathbf{k}}^{-+})^T$  with  $\hat{\varphi}_{\mathbf{k}}^{+-} = (\hat{f}_{\mathbf{k}}^+, (\hat{f}_{-\mathbf{k}}^-)^T)^T$  denoting the electron-hole subspace basis with band index  $(+, -)$  and  $\hat{\varphi}_{\mathbf{k}}^{-+} = (\hat{f}_{\mathbf{k}}^-, (\hat{f}_{-\mathbf{k}}^+)^T)^T$  as the subspace basis with the band index  $(-, +)$ . Thus, we rewrite the superconducting Hamiltonian in the band basis as  $H = \sum_{\mathbf{k}} \hat{\varphi}_{\mathbf{k}}^\dagger \hat{h}(\mathbf{k}) \hat{\varphi}_{\mathbf{k}}$  with

$$\hat{h}(\mathbf{k}) = \begin{pmatrix} E_{\mathbf{k}}^+ & \hat{\Delta}_{\mathbf{k}}^{+-} & 0 & \hat{\Delta}_{\mathbf{k}}^{++} \\ (\hat{\Delta}_{\mathbf{k}}^{+-})^\dagger & -E_{\mathbf{k}}^- & (\hat{\Delta}_{\mathbf{k}}^{-+})^\dagger & 0 \\ 0 & \hat{\Delta}_{\mathbf{k}}^{-+} & E_{\mathbf{k}}^- & \hat{\Delta}_{\mathbf{k}}^{-+} \\ (\hat{\Delta}_{\mathbf{k}}^{++})^\dagger & 0 & (\hat{\Delta}_{\mathbf{k}}^{-+})^\dagger & -E_{\mathbf{k}}^+ \end{pmatrix}, \quad (4)$$

where  $\hat{\Delta}_{\mathbf{k}}^{+-}$  is the projection of the pairing instability onto the inter-band basis given by  $\hat{\Delta}_{\mathbf{k}}^{+-} = \hat{V}_{\mathbf{k}}^{+\dagger} \hat{\mathcal{H}}_\eta^{J,S,L}(\mathbf{k}) (\hat{V}_{-\mathbf{k}}^-)^\dagger$ . Treating the off-diagonal blocks, corresponding to the intra-band pairing denoted by  $\hat{\Delta}_{\mathbf{k}}^{\nu\nu}$  with  $\nu \in \{+, -\}$ , as a perturbation to the inter-band diagonal block and employing the folding down approach [49], we arrive at the effective superconducting Hamiltonian valid in the vicinity of the GLSs

$$H_{\text{eff}}^{+-}(\mathbf{k}) = \begin{pmatrix} E_{\mathbf{k}}^+ + \hat{\varepsilon}_{\mathbf{k}}^{++} & \hat{\Delta}_{\text{eff}}^{+-}(\mathbf{k}) \\ (\hat{\Delta}_{\text{eff}}^{+-}(\mathbf{k}))^\dagger & -E_{\mathbf{k}}^- + \hat{\varepsilon}_{\mathbf{k}}^{--} \end{pmatrix}. \quad (5)$$

The second term on the diagonal in Eq. (5) is a pseudospin energy shift induced by the pairing of intra-band quasi-particles, given by  $\hat{\varepsilon}_{\mathbf{k}}^{\nu\nu} = \hat{\Delta}_{\mathbf{k}}^{\nu\nu} (\hat{\Delta}_{\mathbf{k}}^{\nu\nu})^\dagger / (\omega + \nu E_{\mathbf{k}}^\nu)$  with  $\nu \in \{+, -\}$ . Notably, Eq. (5) is different from a typical BdG Hamiltonian. The effective particle-hole symmetry is broken due to the presence of non-identical diagonal entries arising from the nature of two different energy bands. The inter-band representation of the effective superconducting Hamiltonian takes the form

$$\hat{\Delta}_{\text{eff}}^{+-}(\mathbf{k}) = \hat{\Delta}_{\mathbf{k}}^{+-} + \varepsilon_{\mathbf{k}}^{-1} \hat{\Delta}_{\mathbf{k}}^{++} (\hat{\Delta}_{\mathbf{k}}^{-+})^\dagger \hat{\Delta}_{\mathbf{k}}^{--}, \quad (6)$$

where  $\varepsilon_{\mathbf{k}} = (\omega + E_{\mathbf{k}}^+) (\omega - E_{\mathbf{k}}^-)$  [50]. In the weak-pairing limit, the second term is small close to the GLSs and can be neglected. The superconducting spectrum for the FEE takes the form

$$\mathcal{E}_\pm(\mathbf{k}) = \varepsilon_{\mathbf{k},1} + \varepsilon_{\mathbf{k},2} \pm \sqrt{(\varepsilon_{\mathbf{k},1} - \varepsilon_{\mathbf{k},2})^2 + \hat{\delta}(\mathbf{k})}, \quad (7)$$

where

$$\delta(\mathbf{k}) = \frac{1}{2} \text{Tr} \{ \hat{\Delta}_{\text{eff}}^{+-}(\mathbf{k}) [\hat{\Delta}_{\text{eff}}^{+-}(\mathbf{k})]^\dagger \}, \quad (8)$$

is the magnitude of the GLS indicating superconducting hybridization between inter-band states [51], i.e., pairing of the  $E_{\mathbf{k}}^+$  band formed by  $j = 3/2$  states with the  $E_{\mathbf{k}}^-$  band formed by  $j = 1/2$  states; Tr stands for the trace of the matrix;  $\varepsilon_{\mathbf{k},1} = (1/2)E_{\mathbf{k}}^+ + (1/4)\text{Tr}(\hat{\varepsilon}_{\mathbf{k}}^{++})$  and  $\varepsilon_{\mathbf{k},2} = -(1/2)E_{\mathbf{k}}^- + (1/4)\text{Tr}(\hat{\varepsilon}_{\mathbf{k}}^{--})$ . The width of the GLSs (small oriented arrows in Figs. 1 and 2) around the finite-energy crossing momentum [52] is  $|\mathcal{E}_+(\tilde{\mathbf{k}}) - \mathcal{E}_-(\tilde{\mathbf{k}})| = 2[\delta(\tilde{\mathbf{k}})]^{1/2}$ . Note that the matrix form of  $\hat{\Delta}_{\text{eff}}^{+-}(\mathbf{k})$  depends on the choice of basis while  $\delta(\mathbf{k})$  is a basis-independent observable.

*Symmetry properties.*—Interestingly, the symmetry properties of the finite-energy pairing are different from their low-energy counterpart. For instance, we may witness even(odd)-parity pseudo-spin triplet (singlet) pairing at FEE. This is a direct consequence of the Pauli exclusion principle taking into account the exchange of band-indices in addition to the exchange of spin-indices, i.e.,

$$\hat{\Delta}_{\text{eff}}^{+-}(-\mathbf{k}) = -[\hat{\Delta}_{\text{eff}}^{+-}(\mathbf{k})]^T. \quad (9)$$

In this sense, we can span  $\hat{\Delta}_{\text{eff}}^{+-}(\mathbf{k})$  in the inter-band basis as  $\hat{\Delta}_{\text{eff}}^{+-}(\mathbf{k}) = \mathbf{g}^{+-}(\mathbf{k}) \cdot \boldsymbol{\tau}$ , where the four-component vector  $\mathbf{g}^{+-} = (\mathbf{g}_0^{+-}, \mathbf{g}_x^{+-}, \mathbf{g}_y^{+-}, \mathbf{g}_z^{+-})$  is a complex momentum dependent function,  $\boldsymbol{\tau} = (\tau_0, \tau_x, \tau_y, \tau_z)$  with  $\tau_{x,y,z}$  being the Pauli matrices and  $\tau_0$  the  $2 \times 2$  identity matrix in the inter-band basis. Thus, we obtain the symmetry relations

$$\mathbf{g}_{0,x,z}^{+-}(-\mathbf{k}) = -\mathbf{g}_{0,x,z}^{+-}(\mathbf{k}), \quad \mathbf{g}_y^{+-}(-\mathbf{k}) = \mathbf{g}_y^{+-}(\mathbf{k}). \quad (10)$$

This enables us to directly derive components of the effective inter-band pairing of  $E_{\mathbf{k}}^-$  electron and  $E_{\mathbf{k}}^+$  hole bands denoted by  $\hat{\Delta}_{\text{eff}}^{+-}(\mathbf{k})$ . The  $y$ -component is even in momentum while the other components are odd in momentum [53].

*Pairing channels of  $O_h$  symmetry.*—We apply our theory to all time-reversal symmetric stationary pairing states of cubic point group symmetry up to the  $p$ -wave channel [9, 54] with the aim to identify inter-band pairing. To obtain analytic relations for  $\delta(\mathbf{k})$ , we set  $\gamma = \beta$  ensuring full rotational SO(3) symmetry in the normal state [55]. Note, however, that the pairing states generate cubic anisotropy. The results are summarized in Table I. Remarkably, inter-band pairing is present for a variety of pairing channels. These results can be applied to half-Heusler compounds with appropriate (normal) band structures such as  $RPdBi$  with  $R \in \{Y, Dy, Tb, Sm\}$  [56]. Notably, superconductivity of these materials at low temperatures has already been reported experimentally [29, 36, 39].

$O_h$ ( $T_d$ )	$\eta$	$(J, S, L)$	without ASOC	with ASOC	
$A_{1g}$ ( $A_1$ )	$I$	(0, 0, 0)	×	×	
$A_{1u}$ ( $A_2$ )	$\mathbf{r}$	(0, 1, 1)	×	$[1, 1, 1]^*$	
$T_{1u}$ ( $T_2$ )	$z$	(1, 1, 1)	$[0, 0, 1]$	$[0, 0, 1]$	
$E_g$ ( $E$ )	$3z^2 - r^2$	(2, 2, 0)	$[0, 0, 1]$	✓	
		$x^2 - y^2$	(2, 2, 0)	✓	✓
$E_u$ ( $E$ )	$3z^2 - r^2$	(2, 1, 1)	$[0, 0, 1]^*, k_z = 0$	✓	
		(2, 3, 1)	$[0, 0, 1]$	✓	
		$x^2 - y^2$	(2, 1, 1)	$[0, 0, 1]^*$	$[0, 0, 1]$
		$x^2 - y^2$	(2, 3, 1)	✓	✓
$A_{2u}$ ( $A_1$ )	$xyz$	(3, 3, 1)	$[1, 1, 1]^*$	$[1, 1, 1]^*$	

Table I. Absence/presence of finite-energy Cooper pairing. The first column shows the IR of  $O_h$  ( $T_d$ ) point groups with  $\eta$  denoting the basis label of IR. The third column corresponds to the pairing multiplets of the relative IR. The last two columns indicate presence ✓ (absence ×) of finite-energy Cooper pairing in the entire momentum space in absence and presence of ASOC. The superscript (\*) means that  $\delta(\mathbf{k})$  vanishes in all equivalent directions [57].

First, we observe that the even- and odd-parity spin-singlet pairing states, corresponding to the instability channels  $A_{1g}$  and  $A_{1u}$ , respectively, have vanishing inter-band pairing, i.e.,  $\delta(\mathbf{k}) = 0$  [58]. Contrarily, the cubic spin-triplet state  $T_{1u}$  [9, 59] shows finite inter-band pairing  $\delta(\mathbf{k}) = \Delta^2(k_x^2 + k_y^2)$  with  $\Delta$  being the pairing strength. This indicates that the GLSs are present within the whole momentum space except for the  $[0, 0, 1]$  direction where inter-band pairing vanishes. Next, we focus on Cooper pairing with quintet total angular momentum, i.e.,  $J = 2$ . In this case, the  $J = 2$  state is split by the cubic field into  $E_{g,u} + T_{2g,u}$  where  $E_{g,u}$  ( $T_{2g,u}$ ) is two(three)-dimensional IR. Note that only pairing state labeled by  $E_{g,u}$  corresponds to stationary pairing states of free-energy preserving time-reversal symmetry [9]. The two-fold degenerate components of  $E_{g,u}$  are denoted by  $\eta = (3z^2 - r^2, x^2 - y^2)$ . In the  $j = 3/2$  representation, we find two (four) symmetry allowed pairing channels for even-parity (odd-parity) spin-quintet pairing. For the even-parity states, the quantum number is (2, 2, 0), where the pairing Hamiltonian is momentum independent due to the  $s$ -wave nature of the channel. In this case, the GLSs of the  $3z^2 - r^2$  state are given by  $\delta(\mathbf{k}) = 3\Delta_{\mathbf{k}}^2(k_x^2 + k_y^2)(k^2 + 3k_z^2)$  with  $\Delta_{\mathbf{k}} = \Delta/2k$ , showing non-vanishing pairing of a  $j = 3/2$  electron with a  $j = 1/2$  electron except for the two-fold rotation axis  $[0, 0, 1]$ . Importantly, the  $x^2 - y^2$  state exhibits full GLSs within the entire momentum space.

The odd-parity spin-quintet channel has four momentum dependent stationary pairing states due to  $L = 1$ . The first two states correspond to the  $3z^2 - r^2$  basis having Cooper pair quantum numbers (2, 1, 1) and (2, 3, 1). These states differ only in the intrinsic spin quantum number where  $S = 1$  and  $S = 3$  denote spin dipole and

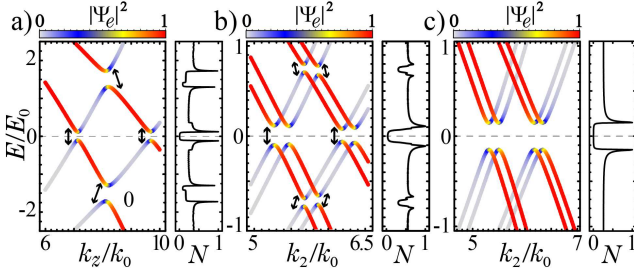


Fig. 2. BdG spectra in (a)  $[0, 0, 1]$  and (b and c)  $[1, 0, 1]$  (with  $k_x = k_z = k_2$  and  $k_y = 0$ ) directions for (a)  $(\Delta/E_0a, \delta/E_0a) = (3.5, 10)$ , (b)  $(1.5, 2.5)$ , and (c)  $(0.15, 2.5)$ , respectively. (a) and (b) correspond to  $xyz$   $p$ -wave spin-septet pairing, and (c) corresponds to  $A_{1g}$   $s$ -wave spin-singlet pairing. The corresponding density of states  $N$  normalized with respect to its maximum value are presented in the right panel of each spectrum.  $\gamma = -0.05|\alpha|$  and other parameters are the same as those in Fig. 1.

octupole moments, respectively. The inter-band GLS for the former state takes the form  $\delta^{\circ}(\mathbf{k}) = 27\Delta_k^2 (k_x^2 + k_y^2)k_z^2$ . Obviously, it vanishes in the  $[0, 0, 1]$  direction (and all equivalent directions [57]) as well as the  $k_z = 0$  plane. For the  $S = 3$  channel, the inter-band GLS becomes

$$\delta^{\circ}(\mathbf{k}) = \Delta_{\mathbf{k}}^2 \sum_i \left[ \zeta_i^{(1)} k_i^4 + \zeta_i^{(2)} k_i^2 k_{i+1}^2 \right], \quad (11)$$

with  $\zeta^{(1)} = (25, 25, 0)$  and  $\zeta^{(2)} = (50, 64, 64)$ . In this case,  $\delta^{\circ}(\mathbf{k})$  is present in the entire momentum space except for the  $z$ -axis.

The inter-band GLSs for the  $p$ -wave  $x^2 - y^2$  state in both  $S = 1$  ( $S = 3$ ) channels can also be described by Eq. (11) with coefficients  $\zeta^{(1)} = (1, 1, 1)$  and  $\zeta^{(2)} = (3, 0, 0)$  ( $\zeta^{(1)} = (25/4, 25/4, 25)$ ,  $\zeta^{(2)} = (103/2, 41, 41)$ ). Hence, the  $S = 3$  channel demonstrates fully GLSs while the  $S = 1$  channel exhibits vanishing  $\delta^{\circ}(\mathbf{k})$  along the  $z$ -axis (and all equivalent axes).

Finally, we look at the spin-septet state denoted by  $A_{2u}$  in the  $O_h$  representation. The Pauli exclusion principle besides the addition of angular momenta imply  $S = 3$  for the  $p$ -wave orbital angular momentum. In this case, the pairing of quasi-particles with different angular momenta manifests itself by

$$\delta^{\circ}(\mathbf{k}) = \frac{3\Delta_{\mathbf{k}}^2}{16} \left\{ \sum_i [4k_i^6 - 3(k_i^4 k_{i+1}^2 + k_i^4 k_{i+2}^2)] + 6k_x^2 k_y^2 k_z^2 \right\}, \quad (12)$$

where  $i+2 = z$  if  $i = x$  and the GLSs are present throughout the  $k$ -space except for the  $[1, 1, 1]$  direction (and all equivalent directions).

*Candidate systems with  $T_d$  structure.*—It is worthwhile to note that the half-Heusler compounds  $RPdBi$  have tetrahedral  $T_d$  symmetry (subgroup of  $O_h$ ) without inversion center. Nevertheless, the formalism of describing the pairing is the same as for the  $O_h$  group but different IR labels apply, *cf.* Table I. The non-centrosymmetry

manifests itself by an antisymmetric spin-orbit coupling (ASOC) given by [6, 60]

$$\hat{H}'(\mathbf{k}) = \delta \sum_i k_i \left( \hat{J}_{i+1} \hat{J}_i \hat{J}_{i+1} - \hat{J}_{i+2} \hat{J}_i \hat{J}_{i+2} \right), \quad (13)$$

where  $\delta$  controls the strength of the ASOC and  $i \in \{x, y, z\}$ . Projection  $\hat{H}'(\mathbf{k})$  into the intra-band basis, this results in splitting the energy-band as  $E_{\mathbf{k}}^{\nu} \rightarrow E_{\mathbf{k}}^{\nu} \pm |g_{\mathbf{k}}^{\nu\nu}|$  with  $g_{\mathbf{k}}^{\nu\nu} \cdot \boldsymbol{\sigma} = \hat{V}_{\mathbf{k}}^{\nu\dagger} \hat{H}'(\mathbf{k}) \hat{V}_{\mathbf{k}}^{\nu}$  and  $\nu = \pm$ , as shown in Figs. 2(b) and 2(c) [61]. Here,  $g_{\mathbf{k}}^{\nu\nu} = (g_x^{\nu\nu}, g_y^{\nu\nu}, g_z^{\nu\nu})$  and  $\boldsymbol{\sigma} = (\hat{\sigma}_x, \hat{\sigma}_y, \hat{\sigma}_z)$  are momentum dependent ASOC vector and Pauli matrices in the intra-band basis, respectively. The lack of inversion symmetry allows the pairing state to be a mixture of even-parity spin-singlet  $\hat{\mathcal{H}}_I^{0,0,0}(\mathbf{k})$  and odd-parity  $p$ -wave states [62]. In this case, the most stable odd-parity pairing state with the largest transition temperature may arise when its  $\mathbf{d}$ -vector aligns parallel to the ASOC vector [63]. Thus, by combining  $\hat{H}'(\mathbf{k})$  with the Cooper pair symmetrization matrix  $\hat{\mathcal{R}} = i\hat{\sigma}_x \otimes \hat{\sigma}_y$  in the  $j = 3/2$  representation, we arrive at the  $p$ -wave spin-septet pairing state  $\hat{\mathcal{H}}_{xyz}^{3,3,1}(\mathbf{k}) = \hat{H}'(\mathbf{k})\hat{\mathcal{R}}$  [6]. The inter-band crossing of the mixed superconducting state  $\hat{\mathcal{H}}_I^{0,0,0}(\mathbf{k}) + \hat{\mathcal{H}}_{xyz}^{3,3,1}(\mathbf{k})$  cannot be hybridized by the inversion symmetry breaking ASOC. Therefore, the emergence of finite-energy superconducting coherence peaks in the DOS are strong indicators of spin-septet pairing demonstrating finite-energy Cooper pairing of quasi-particles with different angular momenta, as shown in Figs. 2(a) and 2(b). Note the difference to the spin-singlet pairing state where the DOS exhibit a flat shape away from the Fermi surface, *cf.* Fig. 2(c). Remarkably, both odd- and even-parity channels of  $3z^2 - r^2$  turn into fully GLSs in the presence of ASOC, *cf.* Table I. This also partially happens for the  $A_2$  state and the  $x^2 - y^2$  state (having quantum number (2,1,1)). Therefore, a small value of ASOC even enhances the likelihood of observing GLSs in the DOS.

*Conclusions.*—We have investigated high-spin Cooper pairing in  $j = 3/2$  superconductors with cubic point-group symmetry. The multiband nature of the system with identical bending configuration allows for observing Cooper pairing away from the Fermi surface in the weak pairing limit. This manifests itself by a pair of indirect finite-energy anti-crossings of BdG bands signaling pairing of quasi-particles having high total angular momenta with quasi-holes possessing lower angular momenta. The phenomenon may be experimentally detectable through tunneling spectroscopy [64–67] and angle-resolved photo-emission spectroscopy [68].

*Note added.*—During the preparation of this manuscript, we became aware of a related proposal of inter-band pairing away from the Fermi surface. This proposal is, however, based on different physical properties and, therefore, applies to different physical systems [69].

We thank S. J. Choi and M. V. Hosseini for fruitful discussions. The work was supported by the DFG (SPP1666 and SFB1170 ToCoTronics), the Würzburg-Dresden Cluster of Excellence ct.qmat, EXC2147, Project Id 390858490, and the Elitenetzwerk Bayern Graduate School on Topological Insulators.

---

\* [masoud.bahari@physik.uni-wuerzburg.de](mailto:masoud.bahari@physik.uni-wuerzburg.de)

- [1] J. Bardeen, L. N. Cooper, and J. R. Schrieffer, *Phys. Rev.* **108**, 1175 (1957).
- [2] J. P. Carbotte, *Rev. Mod. Phys.* **62**, 1027 (1990).
- [3] M. Sigrist and K. Ueda, *Rev. Mod. Phys.* **63**, 239 (1991).
- [4] T.-L. Ho and S. Yip, *Phys. Rev. Lett.* **82**, 247 (1999).
- [5] W. Yang, Y. Li, and C. Wu, *Phys. Rev. Lett.* **117**, 075301 (2016).
- [6] P. M. R. Brydon, L. Wang, M. Weinert, and D. F. Agterberg, *Phys. Rev. Lett.* **116**, 177001 (2016).
- [7] V. Kozii, J. W. F. Venderbos, and L. Fu, *Science Advances* **2**, 10.1126/sciadv.1601835 (2016).
- [8] L. Savary, J. Ruhman, J. W. F. Venderbos, L. Fu, and P. A. Lee, *Phys. Rev. B* **96**, 214514 (2017).
- [9] J. W. F. Venderbos, L. Savary, J. Ruhman, P. A. Lee, and L. Fu, *Phys. Rev. X* **8**, 011029 (2018).
- [10] P. Dutta, F. Parhizgar, and A. M. Black-Schaffer, [arXiv:2106.11983](https://arxiv.org/abs/2106.11983).
- [11] C. Fang, B. A. Bernevig, and M. J. Gilbert, *Phys. Rev. B* **91**, 165421 (2015).
- [12] D. F. Agterberg, P. M. R. Brydon, and C. Timm, *Phys. Rev. Lett.* **118**, 127001 (2017).
- [13] C. Timm, A. P. Schnyder, D. F. Agterberg, and P. M. R. Brydon, *Phys. Rev. B* **96**, 094526 (2017).
- [14] J. Yu and C.-X. Liu, *Phys. Rev. B* **98**, 104514 (2018).
- [15] T. Kawakami, T. Okamura, S. Kobayashi, and M. Sato, *Phys. Rev. X* **8**, 041026 (2018).
- [16] S. Kobayashi, A. Yamakage, Y. Tanaka, and M. Sato, *Phys. Rev. Lett.* **123**, 097002 (2019).
- [17] B. Roy, S. A. A. Ghorashi, M. S. Foster, and A. H. Nevidomskyy, *Phys. Rev. B* **99**, 054505 (2019).
- [18] H. Menke, C. Timm, and P. M. R. Brydon, *Phys. Rev. B* **100**, 224505 (2019).
- [19] S.-T. Tamura, S. Imura, and S. Hoshino, *Phys. Rev. B* **102**, 024505 (2020).
- [20] C. Timm, P. M. R. Brydon, and D. F. Agterberg, *Phys. Rev. B* **103**, 024521 (2021).
- [21] G. Goll, M. Marz, A. Hamann, T. Tomanic, K. Grube, T. Yoshino, and T. Takabatake, *Physica B: Condensed Matter* **403**, 1065 (2008).
- [22] H. Lin, L. A. Wray, Y. Xia, S. Xu, S. Jia, R. J. Cava, A. Bansil, and M. Z. Hasan, *Nature Materials* **9**, 546 (2010).
- [23] S. Chadov, X. Qi, J. Kübler, G. H. Fecher, C. Felser, and S. C. Zhang, *Nature Materials* **9**, 541 (2010).
- [24] N. P. Butch, P. Syers, K. Kirshenbaum, A. P. Hope, and J. Paglione, *Phys. Rev. B* **84**, 220504 (2011).
- [25] T. V. Bay, T. Naka, Y. K. Huang, and A. de Visser, *Phys. Rev. B* **86**, 064515 (2012).
- [26] F. F. Tafti, T. Fujii, A. Juneau-Fecteau, S. René de Cotret, N. Doiron-Leyraud, A. Asamitsu, and L. Taillefer, *Phys. Rev. B* **87**, 184504 (2013).
- [27] Y. Pan, A. M. Nikitin, T. V. Bay, Y. K. Huang, C. Paulsen, B. H. Yan, and A. de Visser, *EPL (Europhysics Letters)* **104**, 27001 (2013).
- [28] G. Xu, W. Wang, X. Zhang, Y. Du, E. Liu, S. Wang, G. Wu, Z. Liu, and X. X. Zhang, *Scientific Reports* **4**, 5709 (2014).
- [29] Y. Nakajima, R. Hu, K. Kirshenbaum, A. Hughes, P. Syers, X. Wang, K. Wang, R. Wang, S. R. Saha, D. Pratt, J. W. Lynn, and J. Paglione, *Science Advances* **1**, 10.1126/sciadv.1500242 (2015).
- [30] A. M. Nikitin, Y. Pan, X. Mao, R. Jeehee, G. K. Araizi, Y. K. Huang, C. Paulsen, S. C. Wu, B. H. Yan, and A. de Visser, *J. Condens. Matter Phys.* **27**, 275701 (2015).
- [31] Z. K. Liu, L. X. Yang, S.-C. Wu, C. Shekhar, J. Jiang, H. F. Yang, Y. Zhang, S.-K. Mo, Z. Hussain, B. Yan, C. Felser, and Y. L. Chen, *Nature Communications* **7**, 12924 (2016).
- [32] M. Meinert, *Phys. Rev. Lett.* **116**, 137001 (2016).
- [33] D. Shrivastava and S. P. Sanyal, *Physica C Supercond.* **544**, 22 (2018).
- [34] H. Kim, K. Wang, Y. Nakajima, R. Hu, S. Ziemak, P. Syers, L. Wang, H. Hodovanets, J. D. Denlinger, P. M. R. Brydon, D. F. Agterberg, M. A. Tanatar, R. Prozorov, and J. Paglione, *Science Advances* **4**, 10.1126/sciadv.aao4513 (2018).
- [35] H. Xiao, T. Hu, W. Liu, Y. L. Zhu, P. G. Li, G. Mu, J. Su, K. Li, and Z. Q. Mao, *Phys. Rev. B* **97**, 224511 (2018).
- [36] S. M. A. Radmanesh, C. Martin, Y. Zhu, X. Yin, H. Xiao, Z. Q. Mao, and L. Spinu, *Phys. Rev. B* **98**, 241111 (2018).
- [37] R. Majumder and M. M. Hossain, *Computational Condensed Matter* **21**, e00402 (2019).
- [38] M. M. Hosen, G. Dhakal, K. Dimitri, H. Choi, F. Kabir, C. Sims, O. Pavlosiuk, P. Wiśniewski, T. Durakiewicz, J.-X. Zhu, D. Kaczorowski, and M. Neupane, *Scientific Reports* **10**, 12343 (2020).
- [39] V. Bhardwaj, A. Bhattacharya, S. Srivastava, V. V. Khovaylo, J. Sannigrahi, N. Banerjee, B. K. Mani, and R. Chatterjee, *Scientific Reports* **11**, 7535 (2021).
- [40] W. Al-Sawai, H. Lin, R. S. Markiewicz, L. A. Wray, Y. Xia, S.-Y. Xu, M. Z. Hasan, and A. Bansil, *Phys. Rev. B* **82**, 125208 (2010).
- [41] A. Jain, S. P. Ong, G. Hautier, W. Chen, W. D. Richards, S. Dacek, S. Cholia, D. Gunter, D. Skinner, G. Ceder, and K. A. Persson, *APL Materials* **1**, 011002 (2013).
- [42] C. Shi, X. Xi, Z. Hou, X. Zhang, G. Xu, E. Liu, W. Wang, W. Wang, J. Chen, and G. Wu, *physica status solidi (b)* **252**, 357 (2015).
- [43] G. Tang, C. Bruder, and W. Belzig, *Phys. Rev. Lett.* **126**, 237001 (2021).
- [44] J. M. Luttinger and W. Kohn, *Phys. Rev.* **97**, 869 (1955).
- [45] G. Dresselhaus, *Phys. Rev.* **100**, 580 (1955).
- [46] M. Tinkham, *Group Theory and Quantum Mechanics*, Dover Books on Chemistry and Earth Sciences (Dover Publications, 2003).
- [47] M. Dresselhaus, G. Dresselhaus, and A. Jorio, *Group Theory: Application to the Physics of Condensed Matter* (Springer Berlin Heidelberg, 2007).
- [48] See the supplemental information for the details on the folding down approach, band basis formalism, and constructing pairing Hamiltonians in cubic point group symmetry. This includes Refs. [6, 8, 9, 14, 19, 46, 47, 49, 59].
- [49] P. Löwdin, *J. Chem. Phys.* **19**, 1396 (1951).

- [50] The analogous model for  $(-+)$  subspace can be derived by substituting  $(+) \leftrightarrow (-)$  in Eq. (5).
- [51] Due to our choice of the pairing basis, the inter-band gap-like structure  $\delta(\mathbf{k})$  is proportional to the identity matrix.
- [52] The band crossings of the FEE appear for the  $C_2$ ,  $C'_2$ , and  $C_3$  axes at  $E = \pm 4|\mu\beta/(4\alpha + 5\beta)|$ ,  $E = \pm 2|\mu/(4\alpha + 5\beta)|\sqrt{\beta^2 + 3\gamma^2}$ , and  $E = \pm 4|\gamma\mu/(4\alpha + 5\beta)|$ , respectively. These crossings constitute the prerequisite for the GLSs.
- [53] In the case of low-energy pairing of intra-band electrons, the usual even(odd)-parity pseudo-spin singlet (triplet) as well as the  $\mathbf{d}$ -vector representation of the odd-parity states [3, 70] can be deduced from  $\hat{\Delta}_{\text{eff}}^{\nu\nu'}(-\mathbf{k}) = -[\hat{\Delta}_{\text{eff}}^{\nu\nu'}(\mathbf{k})]^T$  with  $\nu = \nu' \in \{+, -\}$ . The general form of intra-band pseudo-spin pairing at low energies can be written as  $\hat{\Delta}_{\text{eff}}^{\pm\pm}(\mathbf{k}) = i(\psi(\mathbf{k})\hat{\sigma}_0 + \mathbf{d}(\mathbf{k})\cdot\boldsymbol{\sigma})\hat{\sigma}_y$  where the Pauli matrix vector  $\boldsymbol{\sigma} = (\hat{\sigma}_x, \hat{\sigma}_y, \hat{\sigma}_z)$  is represented in the intra-band basis. Here,  $\psi(\mathbf{k})$  corresponds to the pseudo-spin singlet state and the triplet state is encoded in the  $\mathbf{d}$ -vector  $\mathbf{d}(\mathbf{k}) = (d_x(\mathbf{k}), d_y(\mathbf{k}), d_z(\mathbf{k}))$ . The even(odd)-parity  $\hat{\mathcal{H}}_{\eta}^{J,S,L}(\mathbf{k})$  results in even-parity pseudo-spin singlet (odd-parity pseudo-spin triplet) pairing at  $E = 0$ .
- [54] We expand the electron-electron interaction through the orthogonal basis set of cubic point group symmetry. In this regard, the expanded two-body interaction includes many terms each distinguished by the basis label of cubic symmetry and Cooper pair quantum numbers. We investigate each term, known as the pairing instability channel, individually. In the superconducting phase, one of these channels is dominant which possesses the largest transition temperature. Note that the transition temperature depends on the material dependent parameters of the Hamiltonian.
- [55] For cubic anisotropy in the normal-state  $\gamma \neq \beta$ , our results are still valid. However, the explicit form of  $\delta(\mathbf{k})$  could be dependent on the symmetric spin-orbit couplings.
- [56] For  $R \in \{\text{Dy, Tb}\}(\{Y, \text{Sm}\})$  in  $RPdBi$ , the downward curving spin split  $\Gamma_8$  bands lies close to the Fermi surface. This can be clearly seen for  $YPdBi$  in Refs. [22, 23, 39–42] and for  $R \in \{\text{Dy, Tb, Sm}\}$  in Ref. [41].
- [57] There are three (eight) equivalent directions for the proper two(three)-fold rotation  $C_{2(3)}$  in cubic point group symmetry. The equivalent directions for the  $C_2$  rotation are  $[1, 0, 0]$ ,  $[0, 1, 0]$  and  $[0, 0, 1]$ . For the  $C_3$  rotation, the equivalent directions are  $[1, 1, 1]$ ,  $[\bar{1}, 1, 1]$ ,  $[1, \bar{1}, 1]$ ,  $[1, 1, \bar{1}]$ ,  $[\bar{1}, \bar{1}, 1]$ ,  $[1, \bar{1}, \bar{1}]$ ,  $[\bar{1}, 1, \bar{1}]$  and  $[\bar{1}, \bar{1}, \bar{1}]$ , where  $\bar{1} \equiv -1$ .
- [58] Note that  $g(u)$  stands for even(odd)-parity depending on the symmetry of Cooper pair quantum numbers.
- [59] H. Mäkelä and K.-A. Suominen, *Phys. Rev. Lett.* **99**, 190408 (2007).
- [60] W. Yang, T. Xiang, and C. Wu, *Phys. Rev. B* **96**, 144514 (2017).
- [61] In Fig. 2(a), the two-fold degeneracy along the  $[0, 0, 1]$  direction (and all equivalent directions) is not lifted in the presence of inversion breaking ASOC term. This degeneracy is protected by mirror reflection symmetry and can be witnessed in time-reversal symmetric  $T_d$  crystals [60].
- [62] E. Bauer and M. Sigrist, *Non-Centrosymmetric Superconductors: Introduction and Overview*, Lecture Notes in Physics (Springer Berlin Heidelberg, 2012).
- [63] P. A. Frigeri, D. F. Agterberg, A. Koga, and M. Sigrist, *Phys. Rev. Lett.* **92**, 097001 (2004).
- [64] T. Dvir, F. Masee, L. Attias, M. Khodas, M. Aprili, C. H. L. Quay, and H. Steinberg, *Nature Communications* **9**, 598 (2018).
- [65] Y. Okada, Y. Ando, R. Shimizu, E. Minamitani, S. Shiraki, S. Watanabe, and T. Hitosugi, *Nature Communications* **8**, 15975 (2017).
- [66] R. Kumar, A. Vasdev, S. Das, S. Howlader, K. S. Jat, P. Neha, S. Patnaik, and G. Sheet, *Scientific Reports* **11**, 4090 (2021).
- [67] D. Costanzo, H. Zhang, B. A. Reddy, H. Berger, and A. F. Morpurgo, *Nature Nanotechnology* **13**, 483 (2018).
- [68] M. Hashimoto, I. M. Vishik, R.-H. He, T. P. Devereaux, and Z.-X. Shen, *Nature Physics* **10**, 483 (2014).
- [69] S. Kanasugi and Y. Yanase, [arXiv:2107.07096](https://arxiv.org/abs/2107.07096).
- [70] R. Balian and N. R. Werthamer, *Phys. Rev.* **131**, 1553 (1963).

## Supplemental Material

### Appendix A: Folding-down approach

In this section, we show the derivation of the effective Hamiltonian presented in Eq. (5) of the main paper through the folding down approach [49]. Consider the following Schrödinger equation

$$\begin{pmatrix} \hat{H}_{11} & \hat{H}_{12} \\ \hat{H}_{21} & \hat{H}_{22} \end{pmatrix} \begin{pmatrix} \hat{\psi}_A \\ \hat{\psi}_B \end{pmatrix} = E \begin{pmatrix} \hat{\psi}_A \\ \hat{\psi}_B \end{pmatrix}, \quad (\text{A1})$$

where  $\hat{H}_{ij}$  is a  $n \times n$  sub-block matrix and  $(\hat{\psi}_A, \hat{\psi}_B)^T$  denotes the eigenvector column with  $\hat{\psi}_{A(B)}$  being its sub-block elements. The above eigenvalue problem reduces to the following coupled equations

$$\hat{H}_{11}\hat{\psi}_A + \hat{H}_{12}\hat{\psi}_B = E\hat{\psi}_A, \quad (\text{A2})$$

$$\hat{H}_{21}\hat{\psi}_A + \hat{H}_{22}\hat{\psi}_B = E\hat{\psi}_B. \quad (\text{A3})$$

From Eq. (A3), we obtain  $\hat{\psi}_B$  as

$$\hat{\psi}_B = (E\hat{I}_n - \hat{H}_{22})^{-1}\hat{H}_{21}\hat{\psi}_A, \quad (\text{A4})$$

where  $\hat{I}_n$  is a  $n \times n$  identity matrix. Inserting  $\hat{\psi}_B$  into Eq. (A2) results in

$$\hat{\mathcal{H}}_{\text{eff}} \hat{\psi}_A = E\hat{\psi}_A, \quad (\text{A5})$$

where

$$\hat{\mathcal{H}}_{\text{eff}} = \hat{H}_{11} + \hat{H}_{12}(\omega\hat{I}_n - \hat{H}_{22})^{-1}\hat{H}_{21}. \quad (\text{A6})$$

Note that the second term in  $\hat{\mathcal{H}}_{\text{eff}}$  has the same basis as  $\hat{H}_{11}$ . Moreover, we have taken  $E \rightarrow E - \omega + \omega$  where  $E - \omega \approx 0$  holds in the vicinity of FEE  $\omega$  and making the left hand side of Eq. (A5) independent of  $E$ . The effective low-energy pairing can be easily derived by rearranging the inter-band basis of the sub-block Hamiltonians into the intra-band basis as well as setting  $\omega \approx 0$ .

### Appendix B: Power series expansion

Equation (4) of the main paper can be represented in sub-block matrix formalism as

$$\hat{h}_k = \begin{pmatrix} \hat{h}_{11}(\mathbf{k}) & \hat{h}_{12}(\mathbf{k}) \\ \hat{h}_{21}(\mathbf{k}) & \hat{h}_{22}(\mathbf{k}) \end{pmatrix}, \quad (\text{B1})$$

which allows us to employ Eq. (A6). To perform the power series expansion of  $(\omega\hat{I}_4 - \hat{h}_{22}(\mathbf{k}))^{-1}$ , we follow the subsequent steps. Suppose that we are seeking  $(\hat{A} +$

$\hat{B})^{-1}$  where  $\hat{A}$  and  $\hat{B}$  are invertible Hermitian matrices of dimension  $n$ . Consider the following identity

$$(\hat{A} + \hat{B})^{-1} = \hat{A}^{-1}(\hat{I}_n + \hat{B}\hat{A}^{-1})^{-1}. \quad (\text{B2})$$

A power series expansion of the right hand side of Eq. (B2) reads

$$\begin{aligned} (\hat{I}_n + \hat{B}\hat{A}^{-1})^{-1} &= \sum_{n=0}^{\infty} (-\hat{B}\hat{A}^{-1})^n \\ &= \hat{I}_n - \hat{B}\hat{A}^{-1} + \mathcal{O}(\hat{B}\hat{A}^{-1})^2. \end{aligned} \quad (\text{B3})$$

Inserting the above expansion into the right hand side of Eq. (B2), this results in

$$(\hat{A} + \hat{B})^{-1} \approx \hat{A}^{-1} - \hat{A}^{-1}\hat{B}\hat{A}^{-1}. \quad (\text{B4})$$

Now, expressing  $\omega\hat{I}_4 - \hat{h}_{22}(k)$  in terms of normal  $\hat{\mathcal{E}}_{\mathbf{k}}$  and pairing  $\hat{\Delta}_{\mathbf{k}}$  parts, this results in the following form

$$[\omega\hat{I} - \hat{h}_{22}(\mathbf{k})] = \hat{\mathcal{E}}_{\mathbf{k}} - \hat{\Delta}_{\mathbf{k}} \quad (\text{B5})$$

with

$$\begin{aligned} \hat{\mathcal{E}}_{\mathbf{k}} &\equiv \begin{pmatrix} (\omega - E_{\mathbf{k}}^-)\hat{\sigma}_0 & 0 \\ 0 & (\omega + E_{\mathbf{k}}^+)\hat{\sigma}_0 \end{pmatrix}, \\ \hat{\Delta}_{\mathbf{k}} &\equiv \begin{pmatrix} 0 & \hat{\Delta}_{\mathbf{k}}^{-+} \\ (\hat{\Delta}_{\mathbf{k}}^{-+})^\dagger & 0 \end{pmatrix}. \end{aligned} \quad (\text{B6})$$

Using Eq. (B4), we arrive immediately at

$$[\omega\hat{I} - \hat{h}_{22}(\mathbf{k})]^{-1} \approx \hat{\mathcal{E}}_{\mathbf{k}}^{-1} + \hat{\mathcal{E}}_{\mathbf{k}}^{-1}\hat{\Delta}_{\mathbf{k}}\hat{\mathcal{E}}_{\mathbf{k}}^{-1}, \quad (\text{B7})$$

where we have assumed that  $\hat{\Delta}_{\mathbf{k}}$  in the vicinity of  $\tilde{\mathbf{k}}$  is small. Sandwiching the above term between off-diagonal blocks of Eq. (B1), we arrive at

$$\hat{\Lambda}(\mathbf{k}) = \hat{h}_{12}(\mathbf{k})[\omega\hat{I} - \hat{h}_{22}(\mathbf{k})]^{-1}\hat{h}_{21}(\mathbf{k}), \quad (\text{B8})$$

which read explicitly

$$\hat{\Lambda}(\mathbf{k}) = \begin{pmatrix} \frac{1}{(\omega + E_{\mathbf{k}}^+)} \Delta_{\mathbf{k}}^{++} (\Delta_{\mathbf{k}}^{++})^\dagger & \frac{1}{\varepsilon_{\mathbf{k}}} \Delta_{\mathbf{k}}^{++} (\Delta_{\mathbf{k}}^{-+})^\dagger \Delta_{\mathbf{k}}^{--} \\ \frac{1}{\varepsilon_{\mathbf{k}}} [\Delta_{\mathbf{k}}^{++} (\Delta_{\mathbf{k}}^{-+})^\dagger \Delta_{\mathbf{k}}^{--}]^\dagger & \frac{1}{(\omega - E_{\mathbf{k}}^-)} (\Delta_{\mathbf{k}}^{--})^\dagger \Delta_{\mathbf{k}}^{--} \end{pmatrix}, \quad (\text{B9})$$

where  $\varepsilon_{\mathbf{k}} = (\omega + E_{\mathbf{k}}^+)(\omega - E_{\mathbf{k}}^-)$ . Finally, adding the above term to  $\hat{h}_{11}(\mathbf{k})$ , this results in Eq. (5) of the main paper. In our choice of time-reversal symmetric pairing, the identity  $(\Delta_{\mathbf{k}}^{\nu\nu})^\dagger \Delta_{\mathbf{k}}^{\nu\nu} = \Delta_{\mathbf{k}}^{\nu\nu} (\Delta_{\mathbf{k}}^{\nu\nu})^\dagger$  with  $\nu \in \{+, -\}$ , holds true since  $(\Delta_{\mathbf{k}}^{\nu\nu})^\dagger \Delta_{\mathbf{k}}^{\nu\nu}$  is proportional to the identity matrix.

### Appendix C: Band basis formalism

By exact diagonalization of Eq. (1) of the main text for the case of SO(3) symmetry, i.e.,  $\gamma = \beta$ , we obtain the eigenvector matrix  $\hat{V}_{\mathbf{k}}^{\pm}$  corresponding to the two-fold degenerate eigenvalues  $E_{\mathbf{k}}^{\pm}$  as

$$\hat{V}_{\mathbf{k}}^+ = \Gamma_{\mathbf{k}}^+ \begin{pmatrix} 2k_z k_- / k_+^2 & k_- / k_+ \\ \sqrt{3} k_- / k_+ & 0 \\ 0 & \sqrt{3} \\ 1 & -2k_z / k_- \end{pmatrix}, \quad (\text{C1})$$

and

$$\hat{V}_{\mathbf{k}}^- = \Gamma_{\mathbf{k}}^- \begin{pmatrix} 2\sqrt{3}k_z k_- (k_x^2 + k_y^2) / k_+^2 & -\sqrt{3}k_-^2 \\ -(k + 3k_z^2)(k_x^2 + k_y^2) / k_+^2 & 0 \\ 0 & k + 3k_z^2 \\ \sqrt{3}(k_x^2 + k_y^2) & 2\sqrt{3}k_z k_+ \end{pmatrix}, \quad (\text{C2})$$

where  $\Gamma_{\mathbf{k}}^+ = \sqrt{k_x^2 + k_y^2} / 2k$ ,  $\Gamma_{\mathbf{k}}^- = (2k\sqrt{k + 3k_z^2})^{-1}$ , and  $k_{\pm} = k_x \pm ik_y$ . Note that the eigenvector matrix  $\hat{V} = (\hat{V}_{\mathbf{k}}^+, \hat{V}_{\mathbf{k}}^-)$  is orthonormal (derived by the Gram-Schmidt method) satisfying  $\hat{V}^\dagger \hat{V} = \hat{I}_4$ . The relation between the band basis (pseudo-spin) operator  $\hat{f}_{\mathbf{k}}^{\pm}$  and the fermionic operator is given by

$$\hat{f}_{\mathbf{k}}^{\pm\dagger} = \hat{c}_{\mathbf{k}}^\dagger \hat{V}_{\mathbf{k}}^{\pm}. \quad (\text{C3})$$

The band basis operators should transform under time-reversal and inversion operations as usual fermionic operators. To construct such correspondence, we act with the anti-unitary time-reversal operation  $\Theta$  on the fermionic basis  $c_{\mathbf{k},m}$  in the usual way

$$\Theta c_{\mathbf{k},m_j} = (-1)^{j+m_j} c_{-\mathbf{k},-m_j}, \quad (\text{C4})$$

where the electron annihilation operator acquires a phase in addition to a sign change of momentum and spin quantum number. To perform the above operation on the basis of the normal state Hamiltonian  $\hat{c}_{\mathbf{k},m} = (c_{\mathbf{k},3/2}, c_{\mathbf{k},1/2}, c_{\mathbf{k},-1/2}, c_{\mathbf{k},-3/2})^T$ , we introduce the matrix representation of the time-reversal operator in  $j = 3/2$  basis as  $\hat{\Theta} = \hat{T}\mathcal{K}$  with  $\hat{T} = i\hat{\sigma}_x \otimes \hat{\sigma}_y$  and  $\mathcal{K}$  being the unitary part of the time-reversal operator and the complex conjugate operator, respectively. Therefore, the time-reversal transformation of the normal-state basis takes the form

$$\hat{T}^{-1} \hat{c}_{\mathbf{k}} = \hat{c}'_{-\mathbf{k}}, \quad (\text{C5})$$

where  $\hat{c}'_{-\mathbf{k}}$  is the column of time-reversed fermionic operators given by

$$\hat{c}'_{-\mathbf{k}} = (-c_{-\mathbf{k},-3/2}, c_{-\mathbf{k},-1/2}, -c_{-\mathbf{k},1/2}, c_{-\mathbf{k},3/2})^T. \quad (\text{C6})$$

Note that  $\hat{T}$  fulfills the property  $\hat{T}^2 = -\hat{I}_4$ . Also, the pseudo-spin operator  $f_{\mathbf{k},\uparrow\downarrow}$  under time-reversal operation obeys Eq. (C4) as

$$\hat{\mathcal{T}}^{-1} \hat{f}_{\mathbf{k}}^{\pm} = \hat{f}'_{-\mathbf{k}}^{\pm}, \quad (\text{C7})$$

with  $\hat{\mathcal{T}} = i\hat{\sigma}_y$  denoting the  $2 \times 2$  matrix representation of the unitary part of the time-reversal operator in pseudo-spin-1/2 basis, and

$$\hat{f}'_{-\mathbf{k}}^{\pm} = (-f_{-\mathbf{k},\downarrow}^{\pm}, f_{-\mathbf{k},\uparrow}^{\pm}). \quad (\text{C8})$$

Note that we have taken into account the pseudo-spin index as effective spin-1/2 index. Inserting Eqs. (C7) into Eq. (C5), this results in

$$V'_{-\mathbf{k}} = -\hat{\mathcal{T}} V_{\mathbf{k}}^* (i\sigma_y), \quad (\text{C9})$$

with  $V'_{-\mathbf{k}}$  being the time-reversed matrix of eigenvectors. Moreover, the band basis operators satisfy inversion symmetry as  $\hat{V}_{\mathbf{k}}^{\pm} = \hat{V}'_{-\mathbf{k}}^{\pm}$ .

### Appendix D: Constructing high-spin pairing in $O_h$ symmetry

We start by the density-density interaction decomposed in the pair scattering formalism with the total spin  $S$  in the  $j = 3/2$  basis as

$$H_V = \sum_{\mathbf{k},\mathbf{k}'} \sum_{S,m_S} V(\mathbf{k} - \mathbf{k}') b_{S,m_S}^\dagger(\mathbf{k}) b_{S,m_S}(\mathbf{k}'), \quad (\text{D1})$$

where  $b_{S,m_S}^\dagger(\mathbf{k})$  [ $b_{S,m_S}(\mathbf{k}')$ ] creates (annihilates) a Cooper pair with intrinsic angular momentum  $S$  and spin magnetic quantum number  $m_S$ . The correspondence between the Cooper pair operator and the two-electron state is given by

$$b_{S,m_S}^\dagger(\mathbf{k}) = \sum_{m_1, m_2} \langle j_1, j_2; m_1, m_2 | S, m_S \rangle c_{\mathbf{k},m_1}^\dagger c_{-\mathbf{k},m_2}^\dagger, \quad (\text{D2})$$

where  $\langle j_1, j_2; m_1, m_2 | S, m_S \rangle$  is the Clebsch-Gordan coefficient (CGC) connecting the two-electron state  $|j_1, j_2; m_1, m_2\rangle \equiv c_{\mathbf{k},m_1}^\dagger c_{-\mathbf{k},m_2}^\dagger |0\rangle$  with the Cooper pair state  $|S, m_S\rangle = b_{S,m_S}^\dagger(\mathbf{k}) |0\rangle$ . Here, each electron has total angular momentum  $j$  with relative magnetic quantum number  $m_j$ . For convenience, we can represent the Cooper pair operator in a compact form with the aid of spin multipole matrices [8, 9, 14] as

$$\begin{aligned} b_{S,m_S}^\dagger(\mathbf{k}) &= \hat{c}_{\mathbf{k}}^\dagger [\hat{\mathcal{S}}_{S,m_S} \hat{\mathcal{T}}] (\hat{c}'_{-\mathbf{k}})^\dagger, \\ b_{S,m_S}(\mathbf{k}') &= (\hat{c}'_{-\mathbf{k}'})^T [\hat{\mathcal{S}}_{S,m_S} \hat{\mathcal{T}}]^\dagger \hat{c}_{\mathbf{k}'}, \end{aligned} \quad (\text{D3})$$

where  $\hat{\mathcal{T}}$  plays the role of Cooper pair symmetrization and anti-symmetrization, and  $\hat{\mathcal{S}}_{S,m_S}$  denotes the rank-3 spherical spin-multipole matrices corresponding to the



spin-3/2 representation. Note that the  $\hat{S}_{S,m_S}$  have the properties of spin multipole moments since Cooper pairs are formed with two charges. Hence, they can be classified as spin dipole, quadruple, octupole moments, etc for  $S = 1, 2, 3, \dots$ , respectively. By comparing Eqs. (D2) and (D3), we can conclude that  $\hat{S}_{S,m_S}\hat{T}$  is the matrix of CGCs relating the single particle Cooper pair state to the two electron state. Therefore, to derive the multipole matrices, we must find the highest weight matrix by setting  $m_S = S$  and  $\hat{S}_{S,S} = \hat{C}_{S,S}\hat{T}^{-1}$  where  $C_{S,S}$  is the matrix composed of CGCs. Then, the lower weight spin multipole matrices can be computed by the recursive formula  $[\hat{S}_-, \hat{S}_{S,m_S}] = \hbar\sqrt{S(S+1) - m_S(m_S-1)}\hat{S}_{S,m_S-1}$  where  $\hat{S}_- = \hat{S}_x - i\hat{S}_y$ . Furthermore, the interaction potential  $V(\mathbf{k} - \mathbf{k}')$  can be expanded in terms of spherical harmonics

$$V(\mathbf{k} - \mathbf{k}') = \sum_{L,m_L} \frac{\alpha_L(\mathbf{k}, \mathbf{k}')}{2L+1} Y_{L,m_L}(\mathbf{k}) Y_{L,m_L}^*(\mathbf{k}'). \quad (\text{D4})$$

where the orbital axial angular momentum satisfies the condition  $-L \leq m_L \leq L$  and the coefficient  $\alpha_L(\mathbf{k}, \mathbf{k}')$  can be derived by  $\alpha_L(\mathbf{k}, \mathbf{k}') = \int d\Omega \int d\Omega' \sum_{m_L'} Y_{L',m_L'}^*(\mathbf{k}) Y_{L',m_L'}(\mathbf{k}') V(\mathbf{k} - \mathbf{k}')$ . Here,  $\mathbf{k}$  denotes the norm of momentum vector. Note that the orthogonality of spherical harmonics implies  $\int d\Omega Y_{L',m_L'}^*(\mathbf{k}) Y_{L,m_L}(\mathbf{k}) = \delta_{L,L'} \delta_{m_L,m_L'}$  where  $d\Omega = \sin(\theta) d\theta d\varphi$ . Inserting Eqs. (D3) and (D4) into Eq. (D1), this results in the interaction Hamiltonian in the representation of  $SO(3)$  symmetry

$$H_V^{(L,S)} = \sum' \left[ \hat{c}_{\mathbf{k}}^\dagger (Y_{L,m_L}(\mathbf{k}) \hat{S}_{S,m_S} \hat{T}) (\hat{c}_{-\mathbf{k}}^\dagger)^T \right] \times \left[ (\hat{c}_{-\mathbf{k}'}^T)^T (Y_{L,m_L}(\mathbf{k}') \hat{S}_{S,m_S} \hat{T})^\dagger \hat{c}_{\mathbf{k}'} \right], \quad (\text{D5})$$

where  $\sum' = \sum_{\mathbf{k}, \mathbf{k}'} \sum_{S,m_S} \sum_{L,m_L} [\alpha_L(\mathbf{k}, \mathbf{k}') / (2L+1)]$ . In our system, the total angular momentum  $J$  is a good quantum number. Thus, the density-density interaction in Eq. (D5) should be decomposed in the irreducible representation of total angular momenta. Therefore, the function matrices  $Y_{L,m_L}(\mathbf{k}) \hat{S}_{S,m_S}$  can be transformed into the total angular momentum  $J$  basis by  $Y_{L,m_L}(\mathbf{k}) \hat{S}_{S,m_S} = \sum_{J,m_J} \langle J, m_J | m_L, m_S \rangle \hat{N}_{J,m_J}^{S,L}(\mathbf{k})$  where  $\langle J, m_J | m_L, m_S \rangle$  denotes the CGC connecting the Ket  $|L, S; m_L, m_S\rangle = |L, m_L\rangle \otimes |S, m_S\rangle$  with the Bra  $\langle J, m_J|$ . Note that the  $\hat{N}_{J,m_J}^{S,L}(\mathbf{k})$  indicate the total angular momentum multipole matrices. Eventually, we arrive at the density-density interaction in the representation of  $J$  as

$$H_V^{(J,S,L)} = \sum'' \left[ \hat{c}_{\mathbf{k}}^\dagger (\hat{N}_{J,m_J}^{S,L}(\mathbf{k}) \hat{T}) (\hat{c}_{-\mathbf{k}}^\dagger)^T \right] \times \left[ (\hat{c}_{-\mathbf{k}'}^T)^T (\hat{N}_{J,m_J}^{S,L}(\mathbf{k}') \hat{T})^\dagger \hat{c}_{\mathbf{k}'} \right], \quad (\text{D6})$$

where  $\sum'' = \sum_{\mathbf{k}, \mathbf{k}'} \sum_{J,m_J} \sum_{S,L} [\alpha_L(\mathbf{k}, \mathbf{k}') / (2L+1)]$  and

$$\hat{N}_{J,m_J}^{S,L}(\mathbf{k}) = \sum_{m_L, m_S} \langle m_L, m_S | J, m_J \rangle Y_{L,m_L}(\mathbf{k}) \hat{S}_{S,m_S}. \quad (\text{D7})$$

This filters out magnetic orbital and axial spin angular momenta satisfying  $|m_L + m_S| = m_J$ . Note that for  $L = 1$  we have  $\alpha_{L=1} = 4\pi |\mathbf{k}| |\mathbf{k}'|$ .

In the presence of spherical symmetry, the gap functions are labeled by an infinite number of IRs corresponding to  $SO(3)$  symmetry, i.e., the total angular momentum  $J$ . However, crystals with cubic point group structure have lower symmetry. Therefore, the corresponding pairing instabilities and the corresponding Cooper pair operator must be labeled by the IRs of  $O_h$  symmetry. Thus, we need to derive the cubic representation of  $\hat{N}_{J,m_J}^{S,L}(\mathbf{k})$ . This can be done by the following relation [?] ]

$$\hat{N}_\eta^{J,S,L}(\mathbf{k}) = \sum_{m_1, m_2, m_J} (\hat{O}_\eta \hat{T})_{m_1, m_2} \langle m_1, m_2 | J, m_J \rangle \hat{N}_{J,m_J}^{S,L}(\mathbf{k}), \quad (\text{D8})$$

where  $\eta$  is the basis label of cubic IRs and  $\hat{O}_\eta$  denotes the relative multipole basis matrices in cubic structure normalized to identity, i.e.,  $\text{Tr}(\hat{O}_\eta \hat{O}_\eta^\dagger) = 1$ . The full information about  $O_h$  pairing states and their relative multipole matrices are listed in Table. II. Note that Eq. (D8) shows full correspondence between cubic point group symmetry and  $SO(3)$  symmetry. To obtain the density-density interaction in the cubic field IR, we should replace  $\hat{N}_{J,m_J}^{S,L}(\mathbf{k})$  in Eq. (D6) with  $\hat{N}_\eta^{J,S,L}(\mathbf{k})$  in Eq. (D8). Performing a mean-field approximation with the assumption that the electron pairs have zero center of momentum, we obtain

$$\gamma_{\mathbf{k}}^\dagger \gamma_{\mathbf{k}'} \approx \langle \gamma_{\mathbf{k}}^\dagger \rangle \gamma_{\mathbf{k}'} + \gamma_{\mathbf{k}}^\dagger \langle \gamma_{\mathbf{k}'} \rangle + \langle \gamma_{\mathbf{k}}^\dagger \rangle \langle \gamma_{\mathbf{k}'} \rangle, \quad (\text{D9})$$

where

$$\gamma_{\mathbf{k}}^\dagger \equiv c_{\mathbf{k}, m_1}^\dagger c_{-\mathbf{k}, m_2}^\dagger, \quad (\text{D10})$$

$$\gamma_{\mathbf{k}'} \equiv c_{-\mathbf{k}', m_3} c_{\mathbf{k}', m_4}. \quad (\text{D11})$$

In the above relations, the independency of interaction on spin degrees of freedom requires  $m_1 = m_4$  and  $m_2 = m_3$ . This can be clearly seen by evaluating the matrix element of interaction in two-electron state representation. The mean-field decomposition in Eq. (D9) results in an effective single particle formalism of a cubic pairing Hamiltonian in the channel  $(\eta, J, S, L)$

$$H_\eta^{(J,S,L)} = \sum_{\mathbf{k}} \hat{c}_{\mathbf{k}}^\dagger \hat{\mathcal{H}}_\eta^{J,S,L}(\mathbf{k}) (\hat{c}_{-\mathbf{k}}^\dagger)^T + h.c., \quad (\text{D12})$$

with

$$\hat{\mathcal{H}}_\eta^{J,S,L}(\mathbf{k}) = |\mathbf{k}|^L \Delta_\eta^{J,S,L} \hat{N}_\eta^{J,S,L}(\mathbf{k}) \hat{T}, \quad (\text{D13})$$

where  $\Delta_\eta^{J,S,L}$  denotes the high-spin pairing strength defined by

$$\Delta_\eta^{J,S,L} = \sum_{\mathbf{k}} \langle G | \hat{c}_{-\mathbf{k}}^T (|\mathbf{k}|^L \hat{N}_\eta^{J,S,L}(\mathbf{k}) \hat{T})^\dagger \hat{c}_{\mathbf{k}} | G \rangle. \quad (\text{D14})$$

with  $|G\rangle$  being the superconducting ground state. Note that in the main paper, we have taken the pairing strength as a (small) constant  $\Delta_\eta^{J,S,L} := \Delta$  for all the stationary pairing states in the weak-pairing limit.

### 1. Symmetry properties of inter-band pairing

In this section, we derive Eq. (9) of the main text. The Pauli exclusion principle implies that a sign change in momentum space is accompanied by exchanging the spin indices. This is encoded in  $\hat{\mathcal{H}}_\eta^{J,S,L}(-\mathbf{k}) = -(\hat{\mathcal{H}}_\eta^{J,S,L}(\mathbf{k}))^T$ , therefore,  $\hat{N}_\eta^{J,S,L}(-\mathbf{k})\hat{T} = -(\hat{N}_\eta^{J,S,L}(\mathbf{k})\hat{T})^T$ . Using these relations, we can directly find the symmetry of the inter-band pairing Hamiltonian by projecting Eq. (D13) into the inter-band subspace as

$$\begin{aligned} \hat{\Delta}_{-\mathbf{k}}^{+-} &= \hat{V}_{-\mathbf{k}}^{+\dagger} \left( |\mathbf{k}|^L \Delta_\eta^{J,S,L} \hat{N}_\eta^{J,S,L}(-\mathbf{k}) \hat{T} \right) \hat{V}_{\mathbf{k}}^{-\dagger T} \\ &= -\hat{V}_{-\mathbf{k}}^{+\dagger} \left( |\mathbf{k}|^L \Delta_\eta^{J,S,L} [\hat{N}_\eta^{J,S,L}(\mathbf{k}) \hat{T}]^T \right) \hat{V}_{\mathbf{k}}^{-\dagger T} \\ &= -[\hat{\Delta}_{\mathbf{k}}^{-+}]^T, \end{aligned} \quad (\text{D15})$$

where  $\hat{V}_{-\mathbf{k}}^\pm = \hat{V}_{\mathbf{k}}^\pm$  due to inversion symmetry. In the next sections, we present the explicit form of all symmetry allowed stationary  $s$ - and  $p$ -wave cubic pairings.

### 2. High-spin s-wave pairing in $O_h$ symmetry

The pairing state with s-wave orbital angular momentum is allowed in the even-parity  $A_{1g}$  and  $E_g$  channels. Here, we derive the cubic pairing states corresponding to the relative symmetry allowed quantum numbers  $(J, S, L)$ . The even-parity  $A_{1g}$  state in the channel  $(0, 0, 0)$  and  $E_g$  states in the channel  $(2, 2, 0)$  are given by

$$\hat{N}_I^{0,0,0}(\mathbf{k}) = \hat{\mathcal{N}}_{0,0}^{0,0}(\mathbf{k}), \quad (\text{D16})$$

$$\hat{N}_{3z^2-r^2}^{2,2,0}(\mathbf{k}) = \hat{\mathcal{N}}_{2,0}^{2,0}(\mathbf{k}), \quad (\text{D17})$$

$$\hat{N}_{x^2-y^2}^{2,2,0}(\mathbf{k}) = \frac{1}{\sqrt{2}} \left( \hat{\mathcal{N}}_{2,-2}^{2,0}(\mathbf{k}) + \hat{\mathcal{N}}_{2,2}^{2,0}(\mathbf{k}) \right). \quad (\text{D18})$$

Inserting the above relations into Eq. (D13), this results in the explicit matrix formalism of the pairing Hamiltonians as

$$\hat{\mathcal{H}}_I^{0,0,0}(\mathbf{k}) = \Delta_I^{0,0,0} \begin{pmatrix} 0 & 0 & 0 & 1 \\ 0 & 0 & -1 & 0 \\ 0 & 1 & 0 & 0 \\ -1 & 0 & 0 & 0 \end{pmatrix}, \quad (\text{D19})$$

$J$	$O_h$	$\eta$	$\mathcal{O}_\eta(J)$	Stationary state
0	$A_{1g(u)}$	$I(\mathbf{r})$	$I_4$	✓
1	$T_{1u}$	$x$	$J_x$	×
		$y$	$J_y$	×
		$z$	$J_z$	✓
2	$E_{g,u}$	$3z^2 - r^2$	$3J_z^2 - \mathbf{J}^2$	✓
		$x^2 - y^2$	$J_x^2 - J_y^2$	✓
	$T_{2g,u}$	$xy$	$[J_x J_y]$	×
		$zx$	$[J_z J_x]$	×
		$yz$	$[J_y J_z]$	×
		$xyz$	$[J_x J_y J_z]$	✓
3	$A_{2u}$	$x^3$	$J_x^3$	×
		$y^3$	$J_y^3$	×
		$z^3$	$J_z^3$	×
$T_{2u}$	$z(x^2 - y^2)$	$[J_z(J_x^2 - J_y^2)]$	×	
	$x(y^2 - z^2)$	$[J_x(J_y^2 - J_z^2)]$	×	
	$y(z^2 - x^2)$	$[J_y(J_z^2 - J_x^2)]$	×	

Table II. Time-reversal pairing states in cubic point group symmetry. The first and second columns identify the correspondence between total angular momentum of pairing states and IRs of the  $O_h$  symmetry [46, 47]. The real space basis of each IR is denoted in the third column with their corresponding spin basis in the forth column. Here, the square brackets [...] symmetrize the multipole basis operator  $[\hat{A}\hat{B}] = (\hat{A}\hat{B} + \hat{B}\hat{A})/2!$  and  $[\hat{A}\hat{B}\hat{C}] = (\hat{A}\hat{B}\hat{C} + \hat{A}\hat{C}\hat{B} + \hat{B}\hat{C}\hat{A} + \hat{C}\hat{A}\hat{B} + \hat{C}\hat{B}\hat{A})/3!$ . In the last column, ✓ (×) implies that the pairing state is (is not) the stationary state of the free energy [9].

$$\hat{\mathcal{H}}_{3z^2-r^2}^{2,2,0}(\mathbf{k}) = \Delta_{3z^2-r^2}^{2,2,0} \begin{pmatrix} 0 & 0 & 0 & 1 \\ 0 & 0 & 1 & 0 \\ 0 & -1 & 0 & 0 \\ -1 & 0 & 0 & 0 \end{pmatrix}, \quad (\text{D20})$$

$$\hat{\mathcal{H}}_{x^2-y^2}^{2,2,0}(\mathbf{k}) = \Delta_{x^2-y^2}^{2,2,0} \begin{pmatrix} 0 & 1 & 0 & 0 \\ -1 & 0 & 0 & 0 \\ 0 & 0 & 0 & 1 \\ 0 & 0 & -1 & 0 \end{pmatrix}. \quad (\text{D21})$$

### 3. High-spin $p$ -wave pairing in $O_h$ symmetry

The  $p$ -wave gap functions implies that  $L = 1$ . Therefore, the superconducting gap functions depend linearly on momentum. Since the orbital angular momentum is odd, consequently, the spin part of Cooper pairs should be odd due to Fermi statistics. Therefore, the  $p$ -wave gap functions are odd in momentum implying that  $\hat{\mathcal{H}}_\eta^{J,S,L}(-\mathbf{k}) = -\hat{\mathcal{H}}_\eta^{J,S,L}(\mathbf{k})$ . Taking into account the condition  $|S - L| \leq J \leq |S + L|$ , the odd parity  $p$ -wave Cooper pairing can possess either spin dipole structure  $S = 1$  or spin octupole structure  $S = 3$ . Hence, Cooper pairs can have spin-singlet  $J = 0$ , spin-triplet  $J = 1$ ,

spin-quintet  $J = 2$ , and spin-septet  $J = 3$  total angular momenta. It is worth mentioning that the spin-triplet and septet pairings can only happen in the  $p$ -wave channel. In the following, we obtain the explicit matrix formalism of Hamiltonians describing  $p$ -wave pairings in  $O_h$  point group symmetry. This can be done by inserting Eq. (D8) into Eq. (D13).

a. Spin singlet state  $J = 0$

Here, we derive the odd-parity pairing state  $A_{1u}$ . The symmetry constraint allows for the channel  $(0, 1, 1)$ . The  $J$  representation of the  $A_{1u}$  state and the full matrix formalism of pairing results in

$$\hat{N}_r^{0,1,1}(\mathbf{k}) = \hat{N}_{0,0}^{1,1}(\mathbf{k}),$$

$$\hat{\mathcal{H}}_r^{0,1,1}(\mathbf{k}) = \Delta_r^{0,1,1} \begin{pmatrix} 0 & 0 & -\frac{\sqrt{3}}{2}k_- & \frac{3k_z}{2} \\ 0 & k_- & -\frac{1}{2}k_z & \frac{\sqrt{3}}{2}k_+ \\ -\frac{\sqrt{3}}{2}k_- & -\frac{1}{2}k_z & -k_+ & 0 \\ \frac{3k_z}{2} & \frac{\sqrt{3}}{2}k_+ & 0 & 0 \end{pmatrix}. \quad (\text{D22})$$

b. Spin triplet state  $J = 1$

In the cubic field, the  $J = 1$  state is labeled by the  $T_{1u}$  IR which is a three-fold degenerate state, each denoted by the basis  $\eta = x, y, z$ . Note that only  $\eta = z$  is a stationary state of the free energy preserving time-reversal symmetry [9, 59]. Hence, we focus on it. The total angular momentum representation of this state which lies in the channel  $(1, 1, 1)$  is

$$\hat{N}_z^{1,1,1}(\mathbf{k}) = \hat{N}_{1,0}^{1,1}(\mathbf{k}). \quad (\text{D23})$$

The full matrix of the odd-parity spin-triplet pairing takes the form

$$\hat{\mathcal{H}}_z^{1,1,1}(\mathbf{k}) = \Delta_z^{1,1,1} \begin{pmatrix} 0 & 0 & k_- & 0 \\ 0 & -\frac{2}{\sqrt{3}}k_- & 0 & k_+ \\ k_- & 0 & -\frac{2}{\sqrt{3}}k_+ & 0 \\ 0 & k_+ & 0 & 0 \end{pmatrix}. \quad (\text{D24})$$

c. Spin quintet state  $J = 2$

Here, we derive the odd-parity pairing states with  $E_u$  and  $T_{2u}$  IR corresponding to states with quintet total angular momentum. It is worth mentioning that the  $J$  representation of these IR are the same as Eqs. (D20)-(D21). We represent them for  $(S = 1, L = 1)$  and  $(S = 3, L = 1)$  channels. The pairing Hamiltonian of the former channel

takes the form

$$\hat{\mathcal{H}}_{3z^2-r^2}^{2,1,1}(\mathbf{k}) = \Delta_{3z^2-r^2}^{2,1,1} \begin{pmatrix} 0 & 0 & \frac{\sqrt{3}}{2}k_- & 3k_z \\ 0 & -k_- & -k_z & -\frac{\sqrt{3}}{2}k_+ \\ \frac{\sqrt{3}}{2}k_- & -k_z & k_+ & 0 \\ 3k_z & -\frac{\sqrt{3}}{2}k_+ & 0 & 0 \end{pmatrix}, \quad (\text{D25})$$

$$\hat{\mathcal{H}}_{x^2-y^2}^{2,1,1}(\mathbf{k}) = \Delta_{x^2-y^2}^{2,1,1} \begin{pmatrix} 0 & 0 & -k_+ & 0 \\ 0 & \frac{2}{\sqrt{3}}k_+ & 0 & k_- \\ -k_+ & 0 & -\frac{2}{\sqrt{3}}k_- & 0 \\ 0 & k_- & 0 & 0 \end{pmatrix}. \quad (\text{D26})$$

Moreover, the quintet Hamiltonians with spin octupole  $S = 3$  structures are given by

$$\hat{\mathcal{H}}_{3z^2-r^2}^{2,3,1}(\mathbf{k}) = \Delta_{3z^2-r^2}^{2,3,1} \begin{pmatrix} 0 & 0 & \frac{1}{\sqrt{3}}k_- & -\frac{1}{2}k_z \\ 0 & k_- & -\frac{3}{2}k_z & \frac{1}{\sqrt{3}}k_+ \\ \frac{1}{\sqrt{3}}k_- & -\frac{3}{2}k_z & -k_+ & 0 \\ -\frac{1}{2}k_z & \frac{1}{\sqrt{3}}k_+ & 0 & 0 \end{pmatrix}, \quad (\text{D27})$$

$$\hat{\mathcal{H}}_{x^2-y^2}^{2,3,1}(\mathbf{k}) = \Delta_{x^2-y^2}^{2,3,1} \begin{pmatrix} 5\sqrt{3}k_- & -5k_z & -k_+ & 0 \\ -5k_z & -\sqrt{3}k_+ & 0 & k_- \\ -k_+ & 0 & \sqrt{3}k_- & -5k_z \\ 0 & k_- & -5k_z & -5\sqrt{3}k_+ \end{pmatrix}. \quad (\text{D28})$$

d. Spin-septet state  $J = 3$

The  $p$ -wave spin septet  $J = 3$  state in cubic representation decomposes into  $A_{2u} + T_{1u} + T_{2u}$  IR [46, 47]. In this case, the Cooper pairs have only spin octupole structure  $S = 3$ . The  $A_{2u}$  state [6] is a stationary state [9] and its matrix Hamiltonian is given by

$$\hat{N}_{xyz}^{3,3,1}(\mathbf{k}) = \frac{1}{i\sqrt{2}} \left( \hat{N}_{3,2}^{3,1}(\mathbf{k}) - \hat{N}_{3,-2}^{3,1}(\mathbf{k}) \right), \quad (\text{D29})$$

$$\hat{\mathcal{H}}_{xyz}^{3,3,1}(\mathbf{k}) = \Delta_{xyz}^{3,3,1} \begin{pmatrix} \frac{3}{4}k_- & \frac{\sqrt{3}}{2}k_z & \frac{\sqrt{3}}{4}k_+ & 0 \\ \frac{\sqrt{3}}{2}k_z & \frac{3}{4}k_+ & 0 & -\frac{\sqrt{3}}{4}k_- \\ \frac{\sqrt{3}}{4}k_+ & 0 & -\frac{3}{4}k_- & \frac{\sqrt{3}}{2}k_z \\ 0 & -\frac{\sqrt{3}}{4}k_- & \frac{\sqrt{3}}{2}k_z & -\frac{3}{4}k_+ \end{pmatrix}. \quad (\text{D30})$$

**Appendix E:** Spin multipole matrices

The spin multipole matrix for  $S = 1$  and  $S = 3$  with the highest  $m_S$  quantum numbers are

$$\hat{\mathcal{S}}_{1,1} = \begin{pmatrix} 0 & \frac{-\sqrt{3}}{\sqrt{10}} & 0 & 0 \\ 0 & 0 & \frac{-\sqrt{2}}{\sqrt{5}} & 0 \\ 0 & 0 & 0 & \frac{-\sqrt{3}}{\sqrt{10}} \\ 0 & 0 & 0 & 0 \end{pmatrix}, \quad \hat{\mathcal{S}}_{3,3} = \begin{pmatrix} 0 & 0 & 0 & -1 \\ 0 & 0 & 0 & 0 \\ 0 & 0 & 0 & 0 \\ 0 & 0 & 0 & 0 \end{pmatrix}. \quad (\text{E1})$$

Furthermore, the spherical harmonic for  $L = 1$  are  $|\mathbf{k}|Y_{1,\pm 1} = \mp \sqrt{3/8\pi}k_{\pm}$  and  $|\mathbf{k}|Y_{1,0} = \sqrt{3/4\pi}k_z$ . The spin  $\hat{J}_i$  ( $\hat{S}_i$ ) matrices with  $i \in \{x, y, z\}$  in  $j = 3/2$  basis

are given by

$$\begin{aligned} \hat{J}_x = \hat{S}_x &= \frac{\hbar}{2} \begin{pmatrix} 0 & \sqrt{3} & 0 & 0 \\ \sqrt{3} & 0 & 2 & 0 \\ 0 & 2 & 0 & \sqrt{3} \\ 0 & 0 & \sqrt{3} & 0 \end{pmatrix}, \\ \hat{J}_y = \hat{S}_y &= \frac{\hbar}{2} \begin{pmatrix} 0 & -i\sqrt{3} & 0 & 0 \\ i\sqrt{3} & 0 & -i2 & 0 \\ 0 & i2 & 0 & -i\sqrt{3} \\ 0 & 0 & i\sqrt{3} & 0 \end{pmatrix}, \\ \hat{J}_z = \hat{S}_z &= \frac{\hbar}{2} \begin{pmatrix} 3 & 0 & 0 & 0 \\ 0 & 1 & 0 & 0 \\ 0 & 0 & -1 & 0 \\ 0 & 0 & 0 & -3 \end{pmatrix}. \end{aligned} \quad (\text{E2})$$